ELSEVIER

Journal of Structural Geology 29 (2007) 225–240

JOURNAL OF STRUCTURAL GEOLOGY

www.elsevier.com/locate/jsg

Extensional deformation assisted by mineralised fluids within the brittle-ductile transition: Insights from the southwestern Massif Central, France

Jean-Philippe Bellot [a,b,*]

[a] *Bureau des Recherches Géologiques et Minières (BRGM), BP 6009, REM/MESY, 3 Av. Cl. Guillemin, 45060 Orléans Cedex 2, France*
[b] *Institut des Sciences de la Terre, de l'Eau et de l'Univers (ISTEEM), Univ. Montpellier II, Place Eugène Bataillon, 34095 Montpellier Cedex 05, France*

Received 16 March 2006; received in revised form 10 September 2006; accepted 11 September 2006
Available online 7 November 2006

Abstract

Extensional deformation assisted by mineralized fluids within the brittle-ductile transition is inferred using structural, microstructural and textural investigations applied to the Sarlande shear zone of the southwestern Massif Central, France. The shear zone is a low-angle normal fault that bounds the Meuzac antiform to the south. These structures were formed during the NW-SE-trending synorogenic extension of Middle Carboniferous age. Pre-existing lithologies involved in the shear zone led to partitioning of behaviour and hydrothermal alteration in response to crustal extension and channelling of mineralising fluids. Intense fluid-rock interactions produce softening and weakening reactions induced by alteration of K-feldspar, remobilisation of graphite and rutile, and growth of white micas, chlorite and polymetallic sulphides. Extensional shear deformation and mineralization progressively and concomitantly developed within the brittle-ductile transitional crust (~9–13 km depth). The derived crustal-scale model emphasises the importance of collision which led to the production of large quantities of granite-derived fluids, and the creation of a crustal permeability that drove these fluids near to the brittle-ductile transition. Late orogenic extension associated with fluid-rock interactions led to growth of mineralizing low-angle shear zones and footwall domes. The role of mineralising fluids (fluid pressure) appears to be essential in promoting deformation within the brittle-ductile transition of the extending crust.

Keywords: Fluids; Brittle-ductile transition; Low-angle shear zone; Late orogenic extension; Variscan belt; Massif Central

1. Introduction

The transition zone between upper brittle (elastic-frictional) and lower ductile (viscous plastic) crusts is likely to be particularly important in determining the deformation behaviour that considerably influences the evolution of the lithosphere (e.g., Sibson, 1977; Scholz, 1988; Imber et al., 2001; Holdsworth, 2004). In extending crust, this zone is suspected to be relatively thin and to occur between ~10 and ~15 km (e.g., Sibson, 1977, 1982; Scholz, 1988; Rietbrock et al., 1996; Holdsworth, 2004) but these depths fluctuate, depending on geotherms, crustal thickness, and the mineralogical composition of the crust (e.g., Sibson, 1982; Chester, 1995; Ziegler et al., 1995; Stewart et al., 2000; Gueydan et al., 2003).

Due to contrasting behaviour between upper and lower crusts, their boundary is regarded as a zone where tectonic stresses are transferred (e.g., Chen and Molnar, 1983) and extensional strain concentrated (e.g., Passchier, 1984; Gaudemer and Tapponnier, 1987; Hartz et al., 1994; Roberts, 1998), favouring the growth of detachment faults (e.g., White and White, 1983; Lucchitta, 1990; Hernández Enrile, 1991; Jolivet et al., 1998; Gueydan et al., 2003; Iık et al., 2003) leading to the development of metamorphic core complexes (e.g., Davis and Coney, 1979; Coney, 1980; Davis, 1983; Coney and Harms, 1984; Lister and Davis, 1989; Gautier and Brun, 1994) in the core of which deep-seated rocks are exhumed

* Present address: 4 Place de Brie, 13015 Marseille, France.
E-mail address: jpbellot@wanadoo.fr

0191-8141/$ - see front matter © 2006 Elsevier Ltd. All rights reserved.
doi:10.1016/j.jsg.2006.09.004

(e.g., Kurz and Neubauer, 1996; Johnston et al., 2000; Yan et al., 2003; Tricart et al., 2004; Rossetti et al., 2005). Brittle-ductile shear zones outcropping in the field are, therefore, key structures for study as they can lead to a better understanding of the mechanical behaviour of extending continental lithosphere.

Mechanisms proposed to explain the localisation of deformation within the brittle-ductile zone involve increases in strain-rate (Chester, 1995; Ziegler et al., 1995; Gueydan et al., 2003) and/or reactivation of pre-existing lithological boundaries (Wells, 2001). However, fluid-assisted mechanisms largely influence the strength of the lower part of the brittle crust (e.g., Chester, 1995; Evans and Chester, 1995; Ziegler et al., 1995; Gratier et al., 2003; Hayman et al., 2003), of the ductile crust (Rumble and Spear, 1983; Cox, 1995; Wintsch et al., 1995; Gueydan et al., 2003), and of the brittle-ductile transition (Lost and Bradbury, 1984; Imber et al., 2001; Colletini and Holdsworth, 2004), by producing softening and weakening reactions. Although deformation processes within shear zone can increase porosity and permeability (Rumble and Spear, 1983; Wintsch et al., 1995; Collettini and Holdsworth, 2004), fluid circulation tends to lead to retrograde reaction, reducing strength. Because the lower crust is mainly composed of K-feldspar (e.g. Drake and Righter, 2002), the retrograde reaction involving the breakdown of K-feldspar into white mica is likely to considerably reduce grain size (Stewart et al., 2000) within the brittle-ductile zone. Fluids involved in the retrograde reaction are commonly considered to be metamorphic (Rumble and Spear, 1983) and/or meteoric (Fayon et al., 2004) in origin. However, the discovery of mineralised fluids in extensional structures formed at middle crustal levels (e.g., Craw et al., 1999; Smith et al., 1991; Haeberlin et al., 2004; Kolb et al., 2004) suggests that they may play a role in extensional deformation occurring near to the brittle-ductile transition. This suggests that extensional brittle-ductile shear zones may represent potential sites for economic ore deposits.

The aim of this paper is to present a structural, microstructural and textural analysis of a brittle-ductile, mineralized shear zone (Massif Central, France), and use this as the basis for a model emphasising the essential role of hydrothermal fluids in assisting extensional deformation within the brittle-ductile transitional crust.

2. Geological setting

The South Limousin area belongs to the Variscan belt of western Europe (Fig. 1), which resulted from Palaeozoic convergence and collision between the two major continents Laurentia-Baltica and Gondwana between which were located numerous micro-continents including Avalonia and Armorica (e.g., Ziegler, 1989; Franke, 2000; Matte, 2001). Continent-continent collision took place from the Early Devonian to Early Carboniferous (385–355 Ma) and was marked by polyphase thrust tectonics (D_{1-2}) and Barrovian-type metamorphism (0.7–1.0 GPa/550–650 °C) reflecting crustal thickening by nappe stacking (Guillot, 1981; Floc'h, 1983; Bouchez and Jover, 1986; Girardeau et al., 1986; Burg et al., 1987; Ledru et al., 1994; Roig and Faure, 2000; Bellot, 2004). This event resulted in development of an S_{1-2} regional foliation and L_2 lineation. Thrust tectonics evolved to wrench tectonics during which time quartz diorites and granodiorites (365–345 Ma) were intruded into the basement along the left-lateral Estivaux shear zone and in the hinge of the Tulle antiform (Floc'h, 1983; Roig et al., 1996, 1998).

From the Middle to Upper Carboniferous, late orogenic extension (D_3 and D_4) thinned the stack of nappes (Burg et al., 1994; Faure, 1995; Roig et al., 2002). During the Middle Carboniferous, NW-SE-trending synorogenic extension (D_3) led to the development of an S_3 foliation and L_3 lineation due to Argentat normal faulting (335–337 Ma, white mica $^{40}Ar-^{39}Ar$ dating; Roig et al., 2002), to emplacement of the Millevaches granite in the footwall (332–336 Ma, whole-rock Rb–Sr dating; Monier, 1980), and to growth of the Meuzac antiform in the hanging wall. Within the Meuzac antiform, white mica $^{40}Ar-^{39}Ar$ dates of 333–337 Ma for the pegmatites, 333–340 Ma for the granites, and 334–339 Ma for hydrothermally altered gneisses (Alexandrov, 2000) suggest that Meuzac folding, granite/pegmatite emplacement, and a pervasive hydrothermal alteration were coeval with synorogenic extension (Bellot, 2001). Granite occurs as numerous, very thin (<1 km) sills elongated parallel to the L_3 lineation (Floc'h, 1983; Roig et al., 1998; Bellot, 2001). Because of their orientation, L_2 and L_3 lineations are homoaxial and form at the regional scale a composite L_{2-3} lineation (Fig. 2C). Synorogenic extension is followed by the Upper Carboniferous (315–295 Ma), NE-SW-trending postorogenic extension (D_4) that led to brittle strike-slip faulting (Bellot et al., 2003) and deposition of coal-interbedded conglomerates (Bellot et al., 2005).

3. Ductile-brittle deformation along the Sarlande shear zone

3.1. Regional fabric and crustal permeability

The tectonic fabric on the both sides of the Sarlande shear zone is identical and inherited from collision. The crustal fabric is dominantly $L > S$. The flat-lying planar fabric S_{1-2} (Fig. 2A) is defined by alternating bands of pelitic (two mica-garnet-kyanite-staurolite) and quartz-feldspar compositions from centimeter to crustal scales. The NW-SE-trending linear fabric L_{2-3} (Fig. 2B) is defined by aligned biotite, muscovite, and sillimanite, in addition to stretched eclogite and serpentinite lenses. If we consider that permeability is enhanced parallel to foliation and lineation, the crustal permeability of the studied area favours higher fluid flow into a flat-lying plane and along NW-SE-trending lines.

3.2. Geometry of the Sarlande shear zone

The Sarlande shear zone is marked by 1 km-thick and 55 km-long S_3-L_3 mylonitic zone in which the strike and dip of the rock fabrics change eastwards. To the west, the S_3

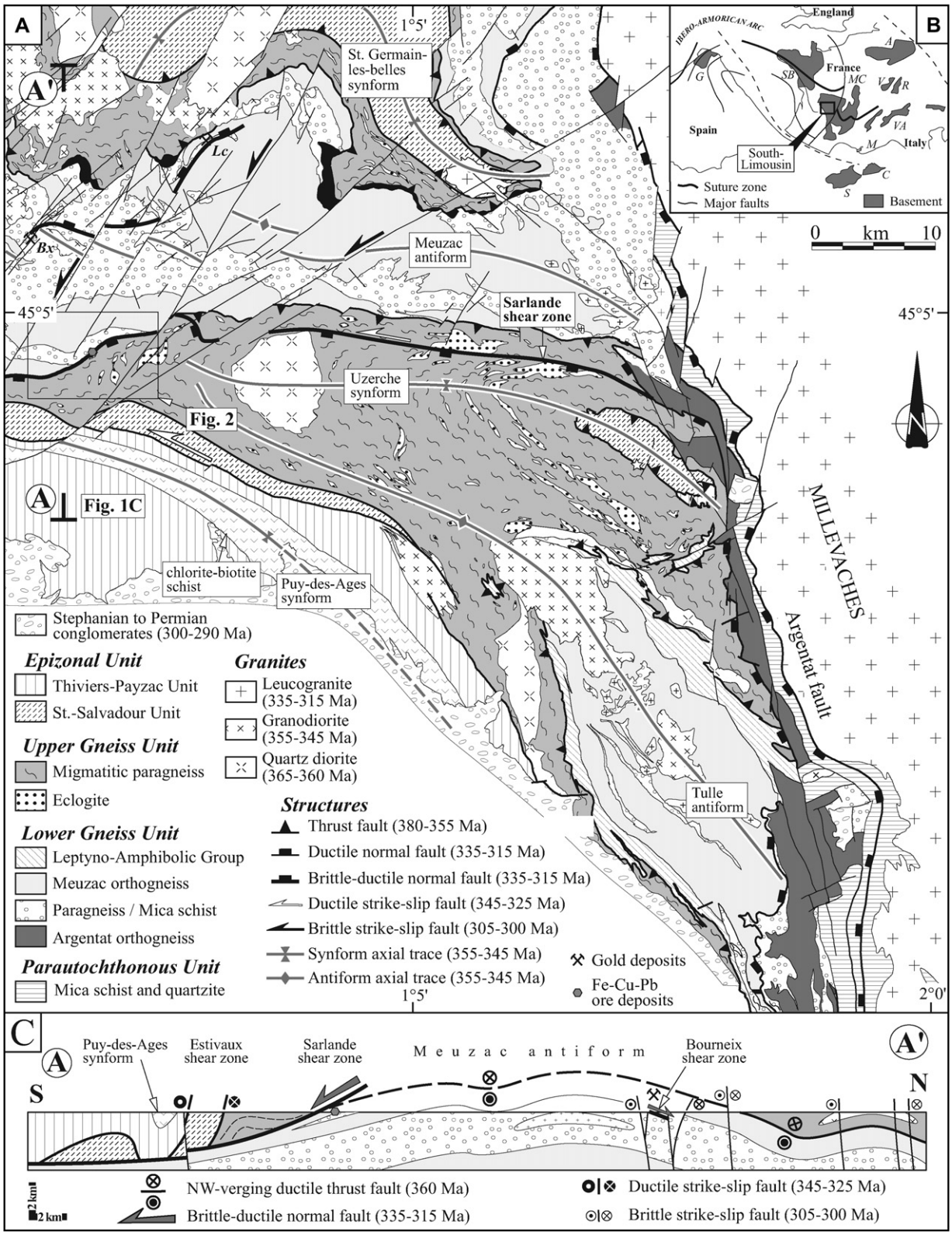

Fig. 1. A. Simplified geological map of the South Limousin area (western Massif Central, France) showing the location of brittle-ductile shear zones and their related syntectonic ore deposits. Sarlande shear zone associated with non-economic Fe-Cu-Pb deposits. Le Bourneix shear zone associated with economic Au deposits. (after Floc'h, 1983 and Bouchot, 1989). Exploited gold deposits (after Bouchot, 1989): Bx = Bourneix; Lc = Leycuras. B. Location of the study area in the context of the Variscan belt of western Europe (after Matte, 2001). Variscan areas: A = Ardennes, C = Corsica, G = Galicia, M = Maures massif, MC = Massif Central, R = Rhenish massif, S = Sardinia, SB = South-Brittany, V = Vosges massif, VA = Variscan Alps. C. Geological cross section showing the close relationships between the Sarlande shear zone and the Meuzac antiform. See Fig. 1A for location.

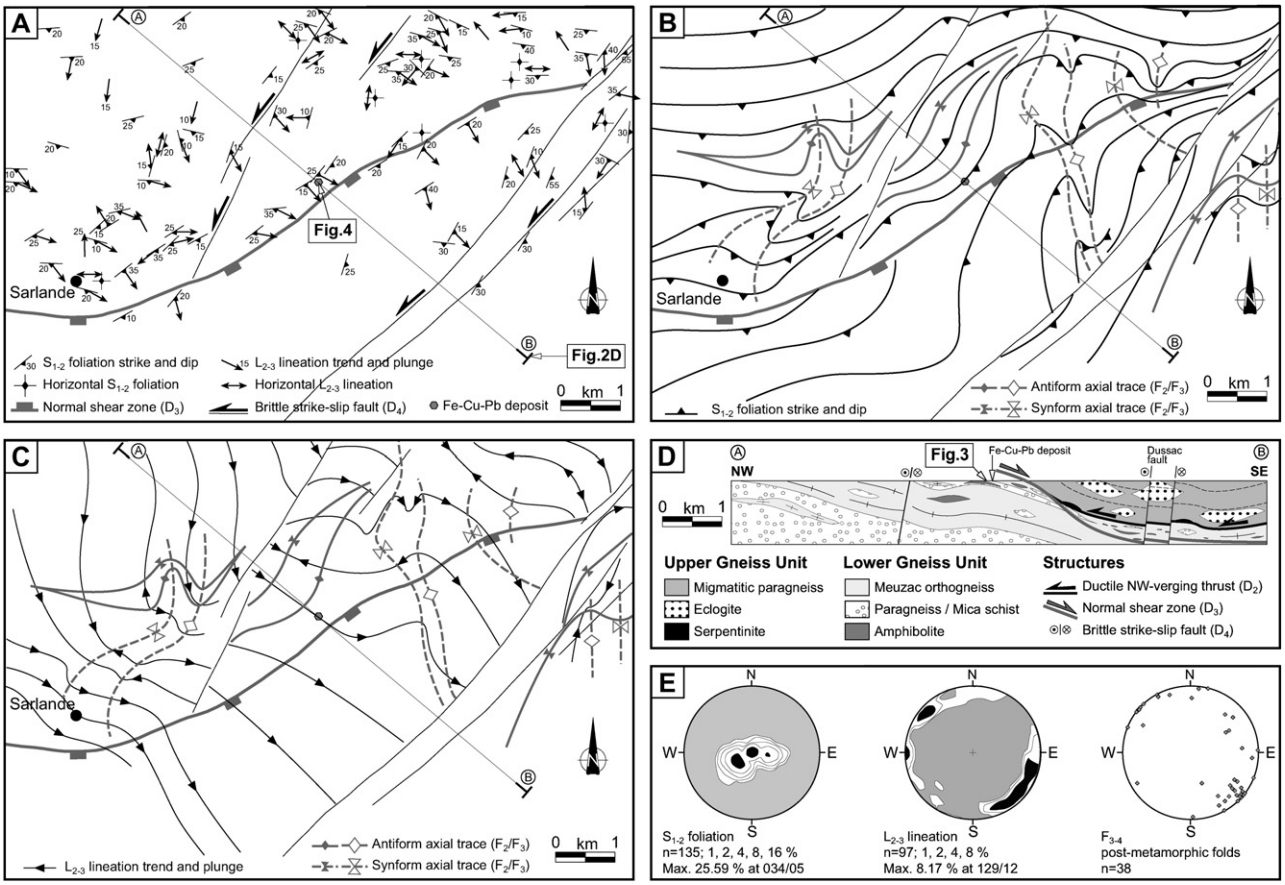

Fig. 2. Structure of basement on both sides of the Sarlande shear zone. A. Map of structural data. See Fig. 1A for location. B. Map of foliation trajectories and fold axial traces. C. Map of lineation trajectories and fold axial traces. Note that L_2 and L_3 lineations are homoaxial and represented as a single, composite L_{2-3} lineation. D. Geological cross section through the Sarlande shear zone. See Fig. 2A for location. E. Equal-area, lower hemisphere, stereographic projections of structural data, with contours representing 1%, 2%, 4%, 8%, and 16% of the total number of measurements per 1% area.

foliation strikes NE-SW and dips gently to the SE. To the east, the S_3 foliation strikes WNW-ESE and dips steeply to the south. In this zone, the S_3 foliation is axial planar of post-metamorphic F_3 open folds which are upright to northeastward verging, and asymmetric. F_3 folds axes trend NW-SE on average and are either horizontal or plunge gently southeastward (Fig. 2E). The largest F_3 fold is the regional-scale Meuzac antiform (Fig. 1). From west to east, the stretching lineation L_3 trends consistently NW-SE (Fig. 2C). These structures are locally reworked by brittle, sinistral strike-slip faults concomitantly developed with F_4 folds (Figs. 2C,D). Although mylonitic rocks and mineralisation textures occur all along the Sarlande shear zone, syntectonic ore deposits and veins are restricted to the western, low-angle, shear zone. Detailed investigations were focussed on the western shear zone where sulphide deposits were discovered.

3.3. Kinematics along the Sarlande shear zone

In the XZ finite strain plane, asymmetric folding of the S_{1-2} foliation on both sides of the Sarlande shear zone suggests a normal movement along the shear zone (Fig. 2D). All along a 1 km-thick level of the lower part of the shear zone, frequent coarse-grained muscovite fish associated with centimetre-scale muscovite shear bands and dynamically recrystallised fine-grained quartz, indicate non-coaxial strain associated with top-to-the SE shearing, corresponding to a normal/sinistral-normal movement along western/eastern parts of the Sarlande shear zone, respectively (Fig. 3). The development of coexisting muscovite fish, with or without undulatory extinction, provide evidence for progressive deformation and muscovite growth during normal shearing.

3.4. Synkinematic minor structures

The shear zone corresponds to a zone of dramatic increase in the intensity of deformation and hydrothermal alteration concentrated along rheological boundaries (orthogneiss/paragneiss) (Fig. 4A). The shear zone includes 10 to 20 cm thick of mylonitic rock displaying grain-size reduction and strong recrystallization, associated with a black to dark gray-coloured alteration. In these so-called ''black mylonites'', the S_3 foliation strikes NE-SW, dips either to the SE or NW, and is associated with slickenlines that trend NW-SE, although decimetre-scale shear planes strike NE-SW and dip steeply southeastward (Fig. 4B). Due to the high proportion of phyllosilicate-bearing fault rocks, the development of cataclasite is restricted to brittlely deformed orthogneiss involved in the

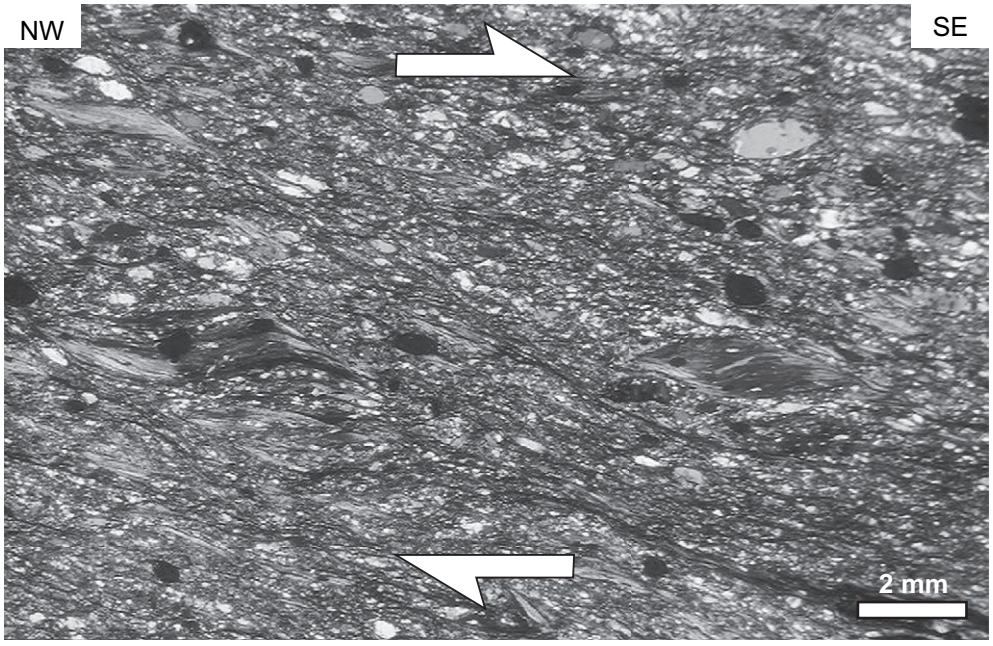

Fig. 3. Photomicrograph of typical ductile mylonite observed along the Sarlande shear zone. See Figs. 2D and 4C for location. Muscovite fish and shear bands indicate non-coaxial strain associated with a top-to-the SE shearing, corresponding to a normal movement along the Sarlande shear zone.

shear zone, as described by Bouchot (1989) in the Bourneix shear zone. Pre-existing contrasts in lithology involved in the shear zone appear to have led to partitioning of behaviour in response to shear deformation (Stewart et al., 2000).

3.5. Competing brittle and viscous deformation processes

3.5.1. Upper part of the shear zone

In the quartz-feldspar-bearing rocks (i.e. orthogneiss) in the upper part of the shear zone, the S_{1-2} foliation is crosscut by high-angle to vertical dipping, dm-long and cm-thick sulphide-bearing veins that grew upwards from the shear zone core (Fig. 4C). These veins formed en echelon arrays that amalgamate into the shear zone. The parallelism between the maximum stretching axis (X) deduced from L_3 lineations of the host-rock, and the minimum stress axis (σ_3), interpreted to be an instantaneous stretching axis, needed to open extensional veins (Fig. 4D), suggests their development in a NW-SE-trending extensional field. The lower ductile part and the middle brittle-ductile part of the shear zone are both devoid of late brittle deformation. These relationships suggest that their development has most likely been coeval with brittle structures of the upper part of the shear zone. These veins are therefore interpreted to be extensional veins developed contemporaneously with disseminated sulphides and shear deformation recognised elsewhere in the Sarlande shear zone. These structures typify brittle strain during shearing.

3.5.2. Centre of the shear zone

In black mylonites in the centre of the shear zone, the geometrical relationships between shear bands and the S_3 foliation, the asymmetric shape of the mylonitic S_3 foliation on both sides of shear bands, and the en echelon pattern of shear planes along the shear zone, all suggest non-coaxial strain associated with a southeastward sense of shear, indicating a normal movement along the shear zone (Fig. 4C). These features typify ductile flow during shear deformation. At the microscopic scale, the en echelon pattern of moderately SE-dipping shear zones with respect to the gently SE-dipping shear zone as a whole confirms its southeastward sense of shear (Figs. 5A,B).

Microscopic-scale shear zones are formed by en echelon short shear planes that preserve a normal movement along individual shear zones. Short shear planes display a variety of low angles with respect to the shear zone and may therefore be interpreted as secondary shears in a Riedel shear model (e.g., Cloos, 1955; Byerlee et al., 1978; Logan et al., 1992). In the Sarlande shear zone, a lack of X and R_2 shears suggests a dominantly non-coaxial strain, although frequent P shears (80%), rare Y shears (15%) and very rare R_1 shears (5%), formed at various levels inside the shear zone suggest moderate amounts of shear strain (Logan et al., 1992). The local development of R_1 and P shears, or P and Y shears in a single microscopic shear zone, argues for progressive shear deformation.

The relay zones between offset short shear planes correspond to pull-apart systems filled by microcrystalline quartz, and interpreted to be dilatational jogs formed at low temperatures (Fig. 5C). Dilatational jogs develop frequently in relays between two P shears or two Y shears, rarely between P and Y shears, never between two R_1 shears or R_1 and P shears. These relationships indicate that the development of dilatational jogs: (1) began at moderate shear strain; (2) is favoured by homogeneous strain in microscopic shear zones; and (3) is associated with progressive deformation. These features, that

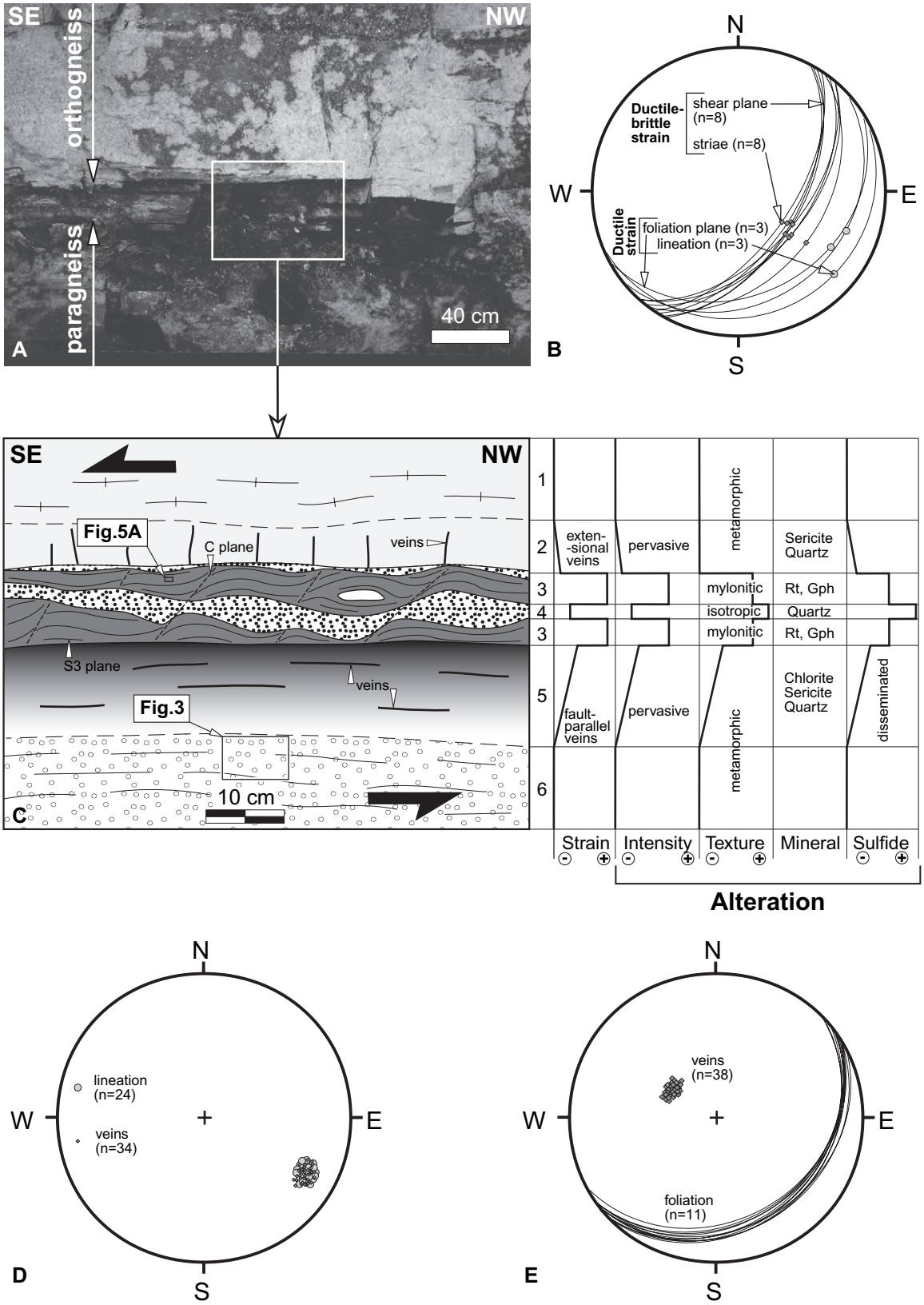

Fig. 4. Field and structural data showing the close relationships between mineralization and brittle-ductile deformation along the Sarlande shear zone. See Figs. 2A and 3C for location. A. Photograph of the shear zone cropping out in the Sarlande area (section normal to the shear zone and parallel to the lineation). B. Equal-area, lower hemisphere, stereographic projections of structural data of the middle part of the shear zone. C. Detailed cross-section of the mineralised shear zone. See Fig. 4A for location. Abbreviations: Rt = rutile, Gph = Graphite. Signification of numbers: 1 = fresh orthogneiss, 2 = altered orthogneiss, 3 = black mylonite (impregnated paragneiss), 4 = sulphide-bearing quartz lens, 5 = altered paragneiss, 6 = fresh paragneiss. D. Equal-area, lower hemisphere, stereographic projections of structural data of the upper part of the shear zone. E. Equal-area, lower hemisphere, stereographic projections of structural data of the lower part of the shear zone.

involve shear rupture, opening, and quartz growth at low temperature, typify brittle strain during shear deformation (e.g. Wibberley et al., 2000).

3.5.3. Lower part of the shear zone

In the quartz-mica-bearing rocks (i.e. paragneiss) in the lower part of the shear zone, sulphide-bearing veins dip parallel to the low-dipping foliation in mylonites (Fig. 4E). These fault-parallel veins typify brittle-ductile strain during shear deformation and mineralization. They are evidence for a dominant fault-parallel displacement and dilatation along the foliation plane that likely results from high fluid pressures. In the lowermost part of the shear zone, muscovite-bearing mylonites are devoid of sulphides (Fig. 3) and indicate ductile flow during shear deformation in the lowermost part of the shear zone.

4. Fluid-rock interaction during the fault activity

The following sections describe how pre-existing contrasting lithologies involved in the shear zone led to partitioning of hydrothermal alteration.

4.1. Upper part of the shear zone: sulphide alteration and extensional veins

In quartz-feldspar-bearing rocks of the upper part of the shear zone, extensional veins are filled by arsenopyrite and pyrite, but cut across disseminated sulphides occurring along foliation-parallel lithological boundaries (Fig. 6A). Both sulphide contents and mineralization textures depend of the protolith of the altered rock, with high contents of disseminated sulphides in quartz-bearing gneiss, and low contents of aggregated sulphides in mica-bearing gneiss (Fig. 6B).

Within the veins, hydrothermal minerals increase in size downwards and are preferentially oriented normal to the veins, i.e. parallel to the NW-SE-trending extension axis. On the vein margins, hydrothermal minerals display a homogeneous fine-grain size, and are not preferentially oriented. These are typical syntaxial veins (Durney and Ramsay, 1973). Close to the veins, paragneiss preserve their metamorphic texture, but a pervasive chlorite-sericite-quartz hydrothermal halo of alteration is observed between sulphides and altered rocks due to the breakdown of syn-D_2 metamorphic minerals into post-D_2, fine-grained assemblage oblique to the previous foliation: garnet and biotite are replaced by chlorite (Fig. 6C), and K-feldspar, plagioclase, and muscovite by sericite (Fig. 6D). The alteration and abundance of sulphides both increase towards the vertical veins.

4.2. Centre of the shear zone: black mylonite-type alteration

Restricted to the centre of the shear zone, the black mylonites correspond to paragneisses strongly deformed and altered by leaching. They are composed of abundant rutile, crystalline graphite, and arsenopyrite, in addition to secondary pyrite, chalcopyrite, and pyrrhotite. Hydrothermal minerals are undeformed, very fine-grained, and strongly oriented parallel to S_3 foliation and C_3 shear planes. These relationships indicate that hydrothermal alteration and shear deformation were likely coeval. These features compare well with other mylonite-hosted sulphides developed in phyllosilicate-bearing rocks deformed close to the brittle-ductile transition in the continental crust (e.g., Bouchot et al., 1989; Porter and Foster, 1991; Hagemann et al., 1994; Cassidy et al., 1998; Allibone et al., 2002; Grocott and Taylor, 2002; McKeagney et al., 2004).

4.3. Centre of the shear zone: quartz-sulphide alteration and lack of deformation

Within the black mylonites, sulphide-bearing quartz lenses, 10 cm-long and 2 cm-thick, are weakly deformed, and correspond to zones of highest hydrothermal alteration and sulphide deposition. Observed minerals are massive pyrite (Fig. 7A), massive sphalerite (Fig. 7B), rutile, and secondary arsenopyrite, chalcopyrite, and pyrrhotite. Sphalerite appears as aggregates of fine-grained crystals elongated parallel to the S_3 foliation and surrounded by very fine-grained quartz deformed at low-temperature (Fig. 7B), indicating that sulphides and deformation were developed coevally. Quartz is homogeneously microcrystalline and preferentially oriented normal to the S_3 foliation. These relationships typify antitaxial veins. Hydrothermal alteration is indicated from muscovite growth at sulphide-quartz boundaries (Fig. 7C), and quartz and chlorite growth between sulphides (Fig. 7D). Coexisting deformed and undeformed hydrothermal minerals likely reflect their growth during progressive deformation (Fig. 7D).

4.4. Geochemical analyses

Geochemical analyses for metallic elements have been performed on 1 dm^3 of the Sarlande and Leycuras black mylonites in order to better characterise hydrothermal alteration. The result emphasizes their similarity, with abundant As (1055/1531 ppm), moderate Sb (116/237 ppm) and Zn (168/188 ppm), little Cu (92/50 ppm), and slight W (15/28 ppm) for Sarlande/Leycuras shear zones. Leycuras black mylonites also include moderate gold (210 ppm) and Pb (192 ppm). The As and Cu contents may reflect the presence of arsenopyrite and chalcopyrite. Sb, Zn, and Pb contents may reflect either the occurrence of infra-microscopic matrix crystals of antimony, sphalerite, and galena, or arsenopyrite enriched in secondary elements. Alternatively, both Sb- and Au-Arsenopyrites have been recognised in the black mylonites of the Bourneix shear zone and may also occur here. Infra-microscopic crystals of antimony, sphalerite, and galena are supposed to exist. These results agree with previous analyses on black mylonites of the Bourneix gold-bearing shear zone (Bouchot, 1989). They indicate that the black mylonites result from intense wall-rock alteration by hydrothermal fluids and preferentially incorporate As, while quartz lenses concentrated other metallic elements, particularly Au, Cu, Pb, and Sb.

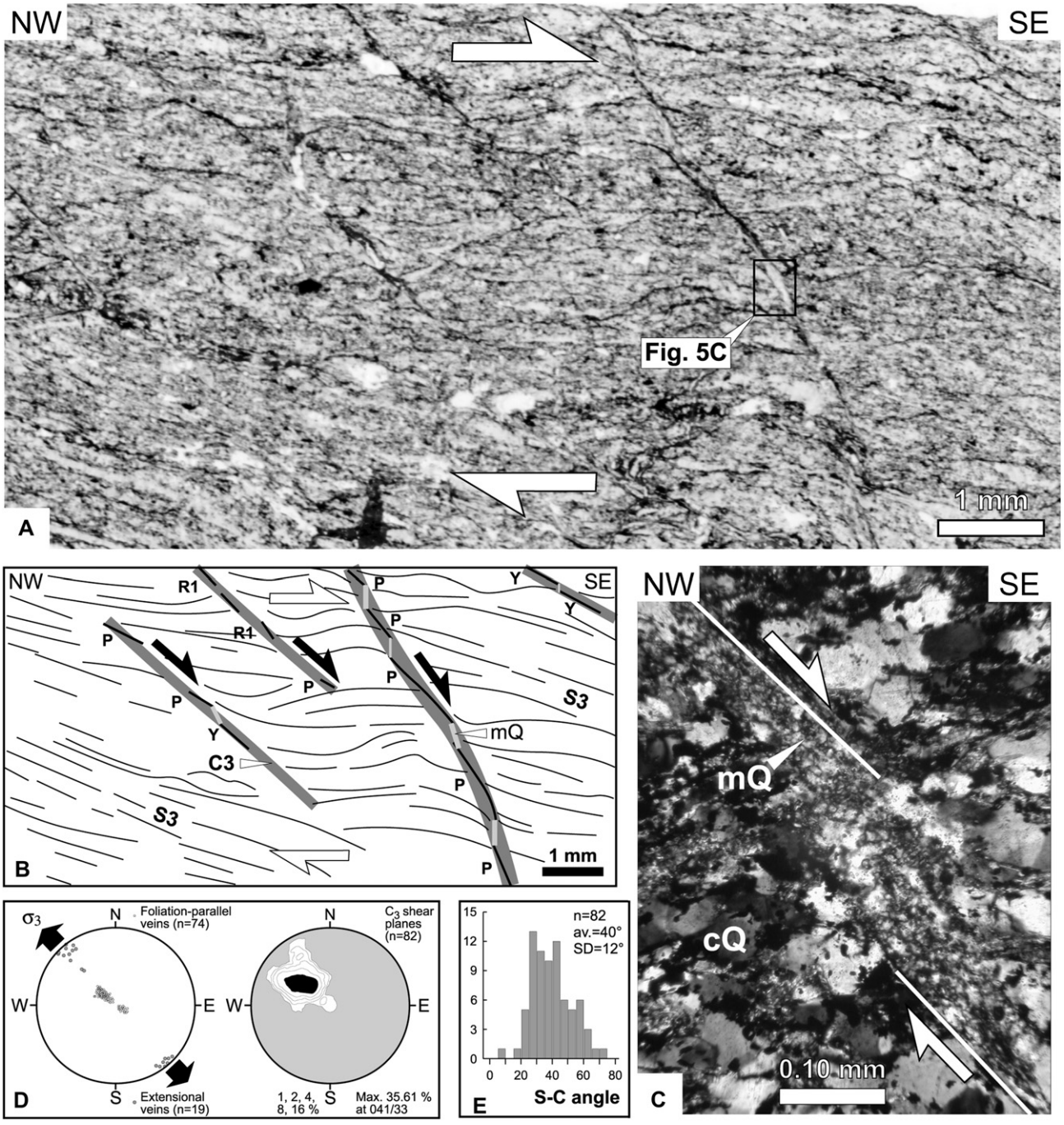

Fig. 5. Microstructural data showing evidence of syntectonic fluid-rock interactions within the black mylonite of the center of the shear zone. See Fig. 4C for location. A. Photomicrograph of the black mylonite. The section is cut perpendicular to the foliation (i.e. vertical), contains the lineation, and parallel to the horizontal (transmitted, plane polarized light). B. Tectonics and kinematics interpretation of the Fig. 5A, showing the coeval development of en echelon short shear planes (interpreted as R_1, P, and Y shears of Riedel) along microscopic shear zones (C3), the mylonitic foliation (S3), growth of microcrystalline quartz (mQ) between short shear planes, and deposition of disseminated sulphide. C. Photomicrograph of microcrystalline quartz filling a pull-apart system developed at the relay of two shear planes (transmitted, cross-polarized light). See Fig. 5A for location. D. Equal-area, lower hemisphere, stereographic projections of orientation of microscopic extensional and foliation-parallel sulphide-bearing veins, and microscopic C3 shear planes of the section of the Fig. 5A. Black arrows indicate, on the left the direction of the minimum stress axis (σ_3), deduced from extensional veins, and on the right the direction of the maximum stretching axis (X) deduced from shear planes. E. Frequency of angles between S_3 and C_3 planes measured on the section of the Fig. 5A. Angles are measured on appropriate sections (normal to the foliation) in order to eliminate any apparent angle effects. The measurement error of $\pm 5^\circ$ corresponds to the local slight variation in the strike of foliation.

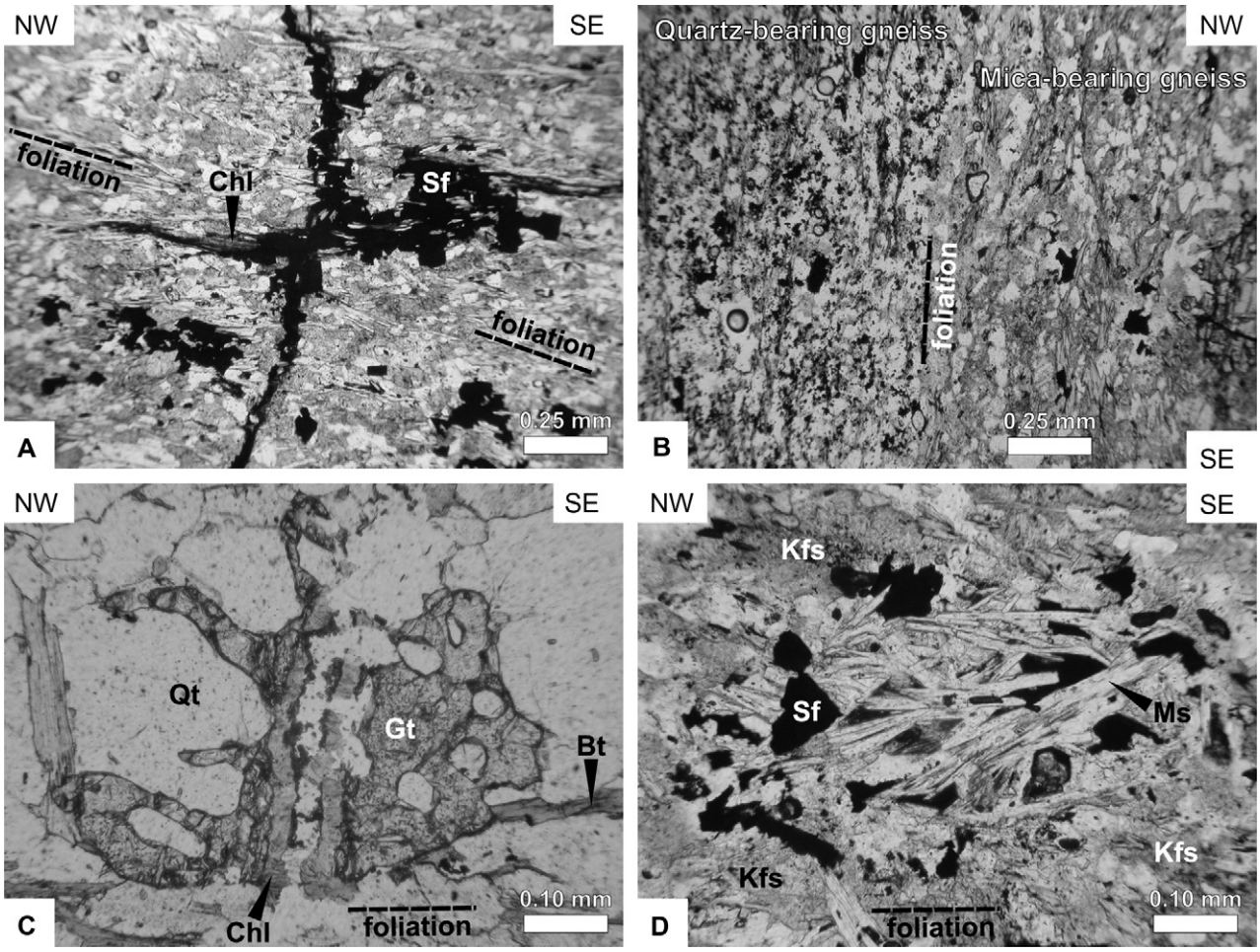

Fig. 6. Photomicrographs of textures in altered gneiss showing syntectonic fluid-rock interactions in the upper part of the Sarlande shear zone (transmitted, plane polarized light). A. Sulphides (Sf: pyrite and arsenopyrite) and chlorite growth in a vertical vein and along the foliation plane cut by veins. B. Contrasting sulphide contents and textures in the shear zone, with high contents of disseminated sulphides in quartz-bearing gneiss, and low contents of aggregate sulphides in mica-bearing gneiss. C. Post-D_2 growth of horizontally-elongated chlorite (Chl) from garnet (Gt) and biotite (Bt) in a vertical vein, suggesting that hydrothermal alteration is associated with a NW-SE-trending extension. D. Post-D_2 muscovite (Ms) growth from K-feldspar (Kfs) due to their reaction with sulphides (Sf).

5. Discussion

5.1. Coeval extensional deformation and mineralization along the Sarlande shear zone

The development of alteration halos parallel to the shear zone suggest that hydrothermal fluids have channelled along the shear zone. Various relationships between the sulphide-bearing quartz lenses and shear planes provide evidence for progressive emplacement of the mineralization during simple shear. The growth of extension veins, fault-parallel veins, and syntectonic assemblages, is indicative of fluid activity in and around the active shear zone. The development of extension veins also indicates high pore fluid pressures. The presented structural, microstructural, and textural analyses therefore point to the coeval development of extensional strain and mineralization along the Sarlande shear zone, in response to a NW-SE extensional strain field. In the Massif Central, this strain field typifies the Variscan synorogenic extension of Middle Carboniferous age (Burg et al., 1994; Faure, 1995; Roig et al., 2002).

5.2. Depth ranges of deformation and mineralization along the Sarlande shear zone

The metamorphic conditions associated with top-to-the SE shear deformation on metapelites located along the Sarlande shear zone have been previously estimated at $P = 0.30$–0.40 GPa and T evolving from 550–650 °C to 300–520 °C (Bellot, 2001). More specifically, chlorite geothermometry applied on altered gneiss in the shear zone yield temperatures ranging from 300 to 430 °C (Vidal et al., 2001). These conditions differ to those of collision-related metamorphism, estimated at 0.50–0.60 GPa/550–650 °C for the region (Floc'h, 1983; Bellot, 2001), and correspond to a post-peak metamorphic event. These values are consistent with the P-T range in which: (1) the arsenopyrite-pyrite-chalcopyrite-sphalerite assemblage is stable (Lusk and Calder, 2004 and references therein); (2) quartz plastically deforms and dynamically recrystallises (>250–300 °C; White, 1976; Schmid and Haas, 1989; Hirth and Tullis, 1994); (3) K-feldspar brittlely deforms under strain (<450–500 °C; Simpson, 1985; Janecke and Evans, 1988; Tullis and Yund, 1992); and (4) the syntectonic

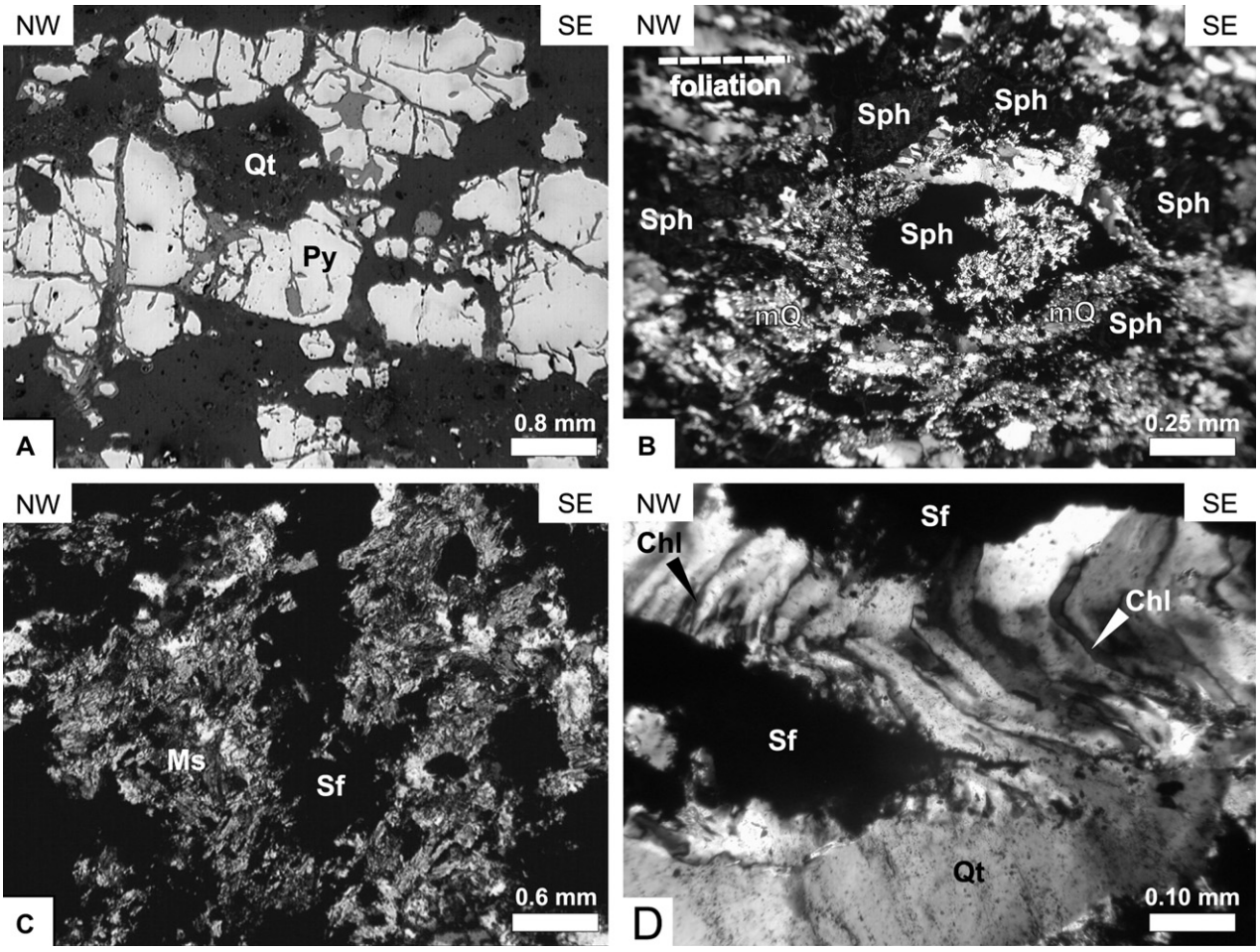

Fig. 7. Photomicrographs of textures in mineralized and altered gneiss showing syntectonic fluid-rock interactions in the center of the Sarlande shear zone. Sections cut normal to the foliation and parallel to the horizontal. A. Massive pyrite (Py) and late quartz (Qt) growth (reflected, plane polarized light). B. Sphalerite (Sph) aggregates elongated parallel to the S_3 foliation, and surrounded by microcrystalline quartz (mQ) deformed at moderate temperature (transmitted, cross-polarized light). This texture indicates that sulphides and deformation developed coevally. C. Muscovite (Ms) growth at the sulphide-quartz boundary (transmitted, cross-polarized light). D. Quartz (Qt) and chlorite (Chl) growth between sulphides (Sf). The deformation of both, indicated by undulose extinction, indicates their emplacement before or during deformation (transmitted, cross-polarized light).

assemblage muscovite-chlorite-quartz is stable in the KFMASH system (250–500 °C; Spear et al., 1999). Assuming a high thermal gradient due to granite emplacement (30 °C/km), a temperature range of 300–430 °C implies depths in the order of 10–14 km.

A similar post-D_2 hydrothermal alteration assemblage of white mica-graphite-pyrite is devoid of shear deformation and has been found extensively in the Meuzac antiform (Bellot, 2001) where altered gneisses and granites display carbonic hydrous fluids (H_2O-CO_2-$CH_4 \pm N_2$-H_2S) which were trapped at P-T conditions evolving from 0.25–0.45 GPa/420–550 °C (Essarraj et al., 2001) to 0.20–0.25 GPa/400–450 °C (Vallance et al., 2004). These conditions are comparable to those of the top-to-the SE shear deformation along the Sarlande shear zone. Moreover, the Middle Carboniferous age of hydrothermal muscovites sampled in the Meuzac antiform (334–339 Ma; Alexandrov, 2000) also typify the Variscan synorogenic extension on a regional scale (Burg et al., 1994; Faure, 1995; Roig et al., 2002). Trapping conditions and the chemical compositions of the fluids suggest a mid-crustal origin (Essarraj et al., 2001).

All available data therefore point to a common crustal depth range of 8–14 km (0.35 ± 0.10 GPa) during shear deformation and ore deposition along the Sarlande shear zone. For quartz-feldspar metamorphic rocks, such pressures correspond to those of the brittle-ductile transition, estimated experimentally at $P \sim 0.30$–0.50 GPa and $T \sim 300$–500 °C (Hirth and Tullis, 1994; Tullis and Yund, 1992). Accordingly, strain along the Sarlande shear zone was accommodated by shear rupture and frictional sliding on the one hand, and by ductile flow on the other hand, and typifies deformation at the brittle-ductile transition, as predicted by field, theoretical and experimental studies of the brittle-ductile transitional zone (Carter and Kirby, 1978; Passchier, 1984; Schmid and Handy, 1991; Passchier and Trouw, 1996). Mica-rich quartz mylonites observed along the Sarlande shear zone (Fig. 3) are very similar to those from the Great Glen Fault Zone (Scotland) which have been interpreted to form by shear deformation and

channelling fluids near to the brittle-ductile transition zone (e.g. Fig. 9 in Stewart et al., 2000).

5.3. Relationships between Sarlande-type shear zones and the Meuzac antiform

In the south Limousin area, other black mylonites are found on the northern flank of the Meuzac antiform close to the Le Bourneix and Leycuras gold deposits (Figs. 1A,C) formed by economic gold-bearing quartz lenses located next to, or at the boundary of black mylonites, although the black mylonites themselves are devoid of gold (Bouchot et al., 1989). According to Bouchot et al. (1989), the northern and southern black mylonites have similar lithologies, types of hydrothermal alteration, and low-angle brittle-ductile structures, and therefore are likely to be the result of a single event. A major difference is that the Le Bourneix and Leycuras mylonites dip (gently) to the NW, and were considered to have originated from a ''NW-SE contraction'' and lately ''reworked by a NW-SE extension'' (Bouchot et al., 1989). An alternative hypothesis is that these sulphide deposits formed during the NW-SE-trending synorogenic extension. In this scheme, the northern Bourneix/Leycuras shear zone may be viewed as a secondary shear zone antithetic to the main southern Sarlande shear zone. Their synchronous development suggests a component of bulk-coaxial strain associated with extensional tectonics. The coeval development of mineralization and shear deformation at a similar crustal depth on both sides of the Meuzac antiform is best explained by a model of doming associated with exhumation of metamorphic rocks and emplacement of aplitic and pegmatitic swarms in the hinge region of the dome hinge during synorogenic extension of the Variscan crust (Fig. 8). Extension and pluton emplacement likely induced a high thermal gradient.

5.4. A crustal model for the Sarlande shear zone

Based on the present data, we propose a crustal model in which extensional deformation is assisted by mineralised fluids at the brittle-ductile transition (Figs. 9A,B). Considerable amounts of monzogranite and granodiorite emplaced during collision are thought to have accumulated near to the roof of the Parautochthonous Unit (Bellot, 2001). They led to the production of numerous, small sills of leucogranites in Upper and Lower Gneiss Units (Fig. 9A). Because of their size, leucogranite bodies cannot reach shallow crustal levels and flatten significantly upon emplacement at mid-crustal levels (8–15 km depth) (Burov et al., 2003). Due to their emplacement into a relative cold basement, leucogranites discharged their pegmatitic phases including aqueous, hydrothermal, and mineralizing fluids (Floc'h, 1983). Hot fluids able to ascend within the ductile crust recharged the system from below and induced a continuous fluid flow (Cox, 2002). They were likely accumulated near to the mechanical boundary between the brittle and ductile crust. Accumulation and lateral migration of fluids likely formed a rather continuous sub-horizontal zone of hydrothermal fluids. The crustal rock fabric, inherited from collisional tectonics, strongly controlled the three dimensional distribution of fluid flow: fluid moved upward vertically parallel to the Z axis then migrated horizontally parallel to the X axis (Fig. 9A). Zones of highest fluid pressure were created at the base of the transitional crust either where fluid accumulated, i.e. the zones where vertical fluid flow stopped, and/or where two horizontal fluid flows converged. It is suggested that the zones of highest fluid pressure drove the nucleation of normal shear planes.

The development of the fluid accumulation zone is associated with the progressive, upward, intense hydrothermal alteration of K-bearing rocks producing K-feldspar breakdown into white mica. This phase change concentrated near the brittle-ductile transition likely led to considerable reductions in the strength of the rocks (Rumble and Spear, 1983; Wintsch et al., 1995), favouring the localisation of deformation into this region (Gueydan et al., 2003). However, deformation began only when fluid impregnation into the transitional zone was sufficiently high to significantly reduce crustal strength. In a tectonic setting of crustal-scale horizontal extension, these mechanical features favour simple shear-dominated deformation and the growth of low-angle (10–25°) shear zones (Gueydan et al., 2003). The anisotropic behaviour of the crust also

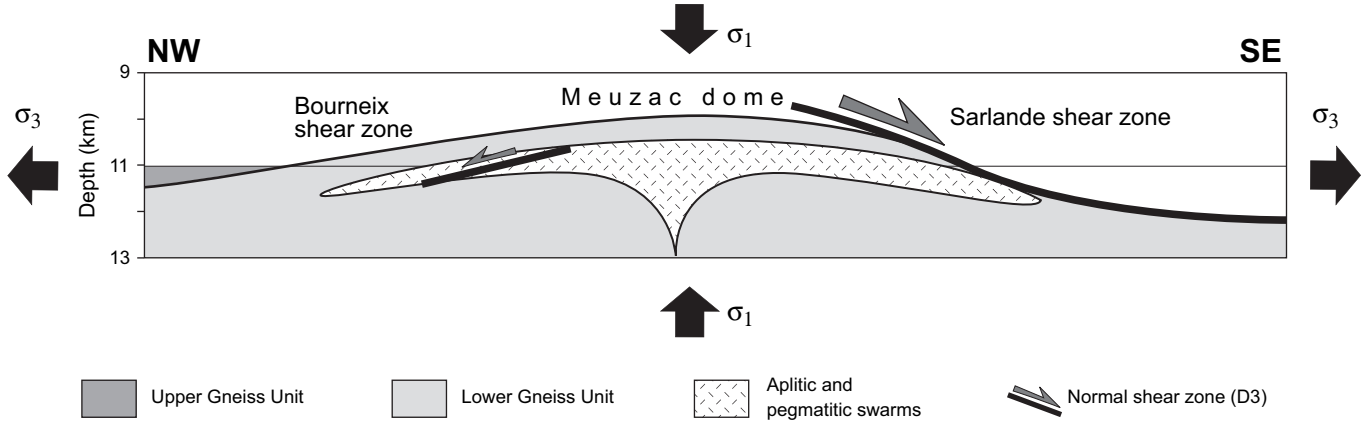

Fig. 8. Interpretative cross-section showing the coeval development of normal shearing along Sarlande and Bourneix faults, doming and granite emplacement within the Meuzac antiform, and channelling of hydrothermal fluids, in response to the Variscan NW-SE-trending extension of Middle Carboniferous age.

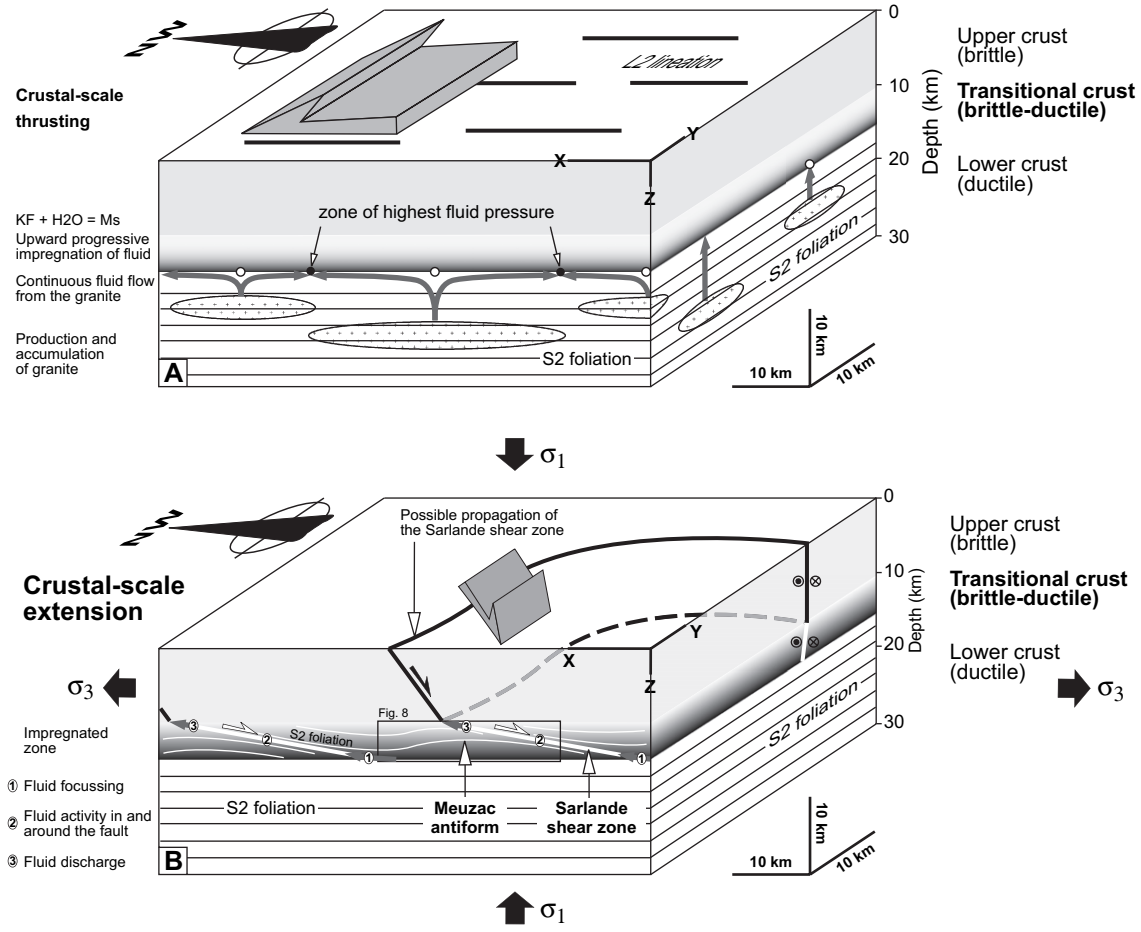

Fig. 9. Crustal-scale model emphasising the key role of mineralizing fluids in assisting extensional deformation near the brittle-ductile transition. A. Pre-extension stage. Mineralising fluids were produced from middle crustal granites and accumulated within the brittle-ductile crust. The model assumes a homogeneous crustal thickness and a homogeneous composition for both upper and lower crusts, allowing the development of a continuous and horizontal brittle-ductile transitional zone. B. Extension stage permitting growth of brittle-ductile shear zones and footwall domes. Granites in the middle crust are omitted for clarity.

favoured the preferential growth of low-angle normal faults (Hanmer et al., 1996). Development of these structures may be interpreted to result from the reactivation of a weak fluid-rich brittle-ductile transition as a low-angle shear zone (Reynolds and Lister, 1987; Axen, 1992; Collettini and Barchi, 2002). It may have been achieved during a relatively short span of time (<1 Ma), with only low differential stresses required for faulting (Gueydan et al., 2003).

5.5. *Progressive deformation and mineralization during Sarlande shear zone growth*

Progressive mineralization and deformation is inferred from: (1) within black mylonites, the development of the sulphide-bearing quartz lenses prior, during, and after shearing (Fig. 4C); (2) in the sulphide-bearing quartz lenses, the preservation of coexisting deformed and undeformed syntectonic hydrothermal minerals (Fig. 7D); and (3) in the lower part of the shear zone, coexisting deformed and undeformed syntectonic muscovites (Fig. 3). The model of progressive mineralization and deformation along the Sarlande extensional shear zone presented in Fig. 10 therefore best explains the observations and data presented here. At a depth of 8–14 km, tectonically-produced horizontal extension, sub-lithostatic pressure, and pore fluid pressure of hydrothermal origin probably acted on a low-angle (~20°) rheological boundary. Because the permeable structure is inclined at low angles to the regional fluid pathways, fluid focussing and input occurred at the higher pressure levels of the shear zone (bottom), whereas fluid discharge occurred in the lower pressure levels (top) of the shear zone (Cox, 2002). The infiltration of hydrothermal fluids into the shear zone likely resulted in contrasting fluid-rock interactions.

In the upper part of the shear zone (i.e. orthogneiss), large-scale units of orthogneiss likely formed barriers for fluids, leading to the development of high fluid pressures at their boundaries with the paragneisses. An increase in the pore fluid factor at a rate more rapid than the increase in shear stress would lead to the progressive opening of vertical veins (Fig. 10) (Cox, 2002 and references therein). Brittle failure of the orthogneiss may also be favoured by concentration of carbonic fluids at the roof of the shear zone which locally increased fluid pressure, as described by Wawrzyniec et al. (1999) in the Simplon fault zone.

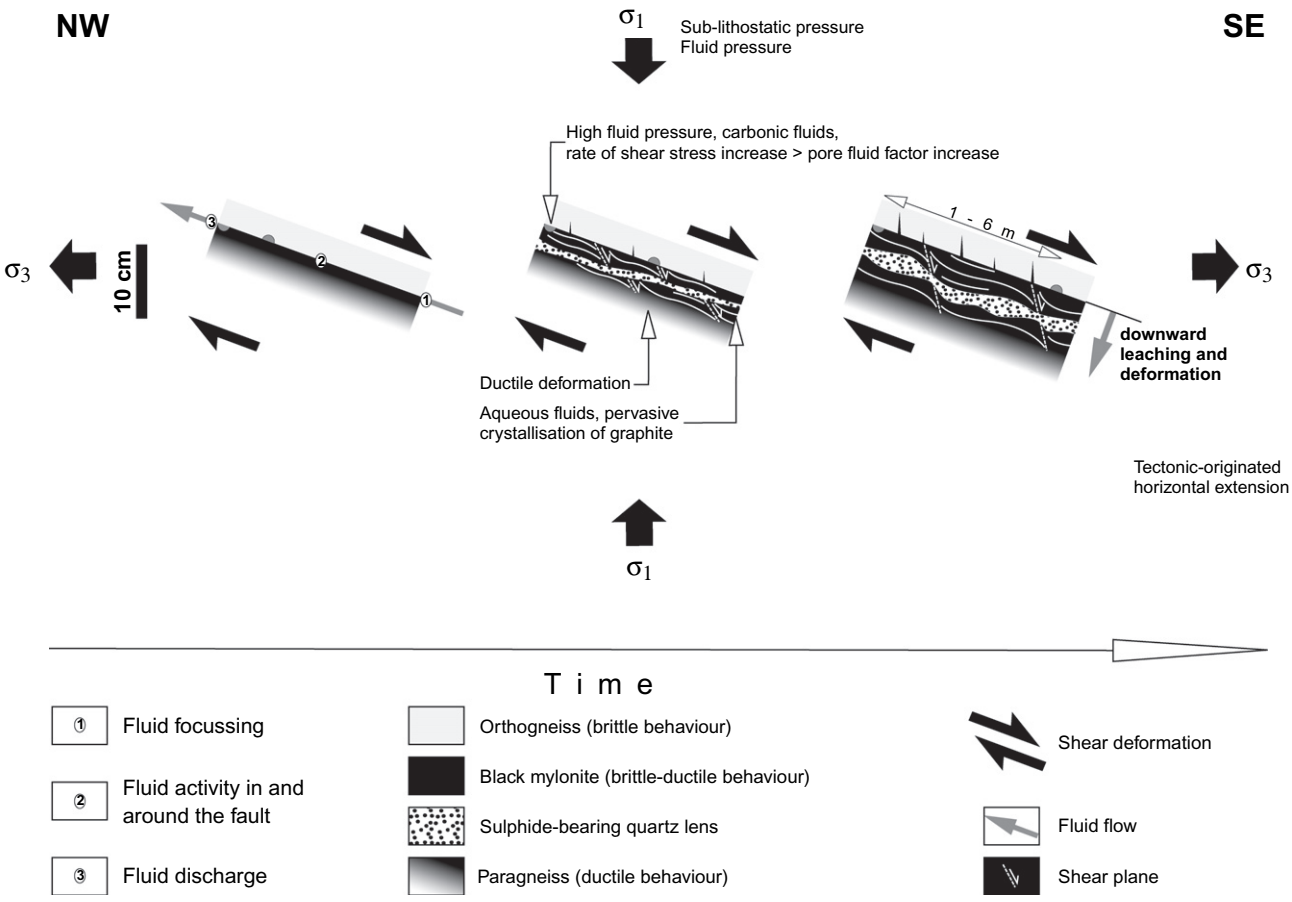

Fig. 10. Model of progressive deformation and mineralization near the brittle-ductile transition (8–14 km depth) proposed to explain the development of the Sarlande shear zone. Vertical scale exaggerated for clarity.

In the lower part of the shear zone (i.e. paragneisses), pervasive fluid-rock interactions have led to K-feldspar breakdown to muscovite (Rumble and Spear, 1983; Wintsch et al., 1995), favouring shear deformation and leaching of the mica-bearing gneisses along the low-dipping foliation plane. The resulting black mylonites grew by progressive, downward deformation and leaching of mica-bearing gneisses, although vertical veins in the upper part of the shear zone grew upward and laterally. The distribution of high fluid fluxes and high pore fluid factors in the shear zone networks has probably driven the growth of the shear zone and its possible propagation to higher crustal levels (Cox et al., 1987, 2001; Sibson, 1996). Aqueous fluids that impregnated most of the paragneiss have allowed ductile deformation to persist to low-pressures and temperatures, as described by Wawrzyniec et al. (1999) in the Simplon fault zone. Pervasive crystallisation of graphite from carbonic hydrothermal fluids within paragneiss also favours a ductile behaviour of these rocks under lower temperature conditions. Within the centre of the shear zone, shear planes progressively grow by developing short microscopic R_1 shears and then P shears. Relays between P shears concentrated high fluid pressure zones that led to opening by shear fracture, filling these regions with non-oriented microcrystalline quartz (Fig. 10). Cooling, due to uplift and/or fluid-rock interactions, led to quartz precipitation and sulphide deposition.

In the lowermost part of the shear zone (i.e. paragneiss), intense interactions between K-bearing hydrothermal fluids and sheared paragneiss led to syn-tectonic muscovite crystallisation within the mylonitic foliation and the development of shear bands.

5.6. Importance of extensional brittle-ductile shear zones in the Variscan belt

In the Variscan basement of Sardinia, economic As-Pb-Fe sulphide deposits with minor occurrences of native gold and silver are hosted by black mylonites included in a 3-km-thick shear zone interpreted as a SW-verging thrust fault (Conti et al., 1998) and recently re-interpreted as a SW-dipping normal fault (Conti et al., 2001). The shear zone bounds a large, orogen-parallel dome. The original slip direction (NW) of the normal fault, after correction of the post-Permian anticlockwise rotation (70°) of Sardinia (Gattacceca, 2001), typifies the strain field of the Variscan synorogenic extension. The related As-Pb-Fe sulphide deposits, previously interpreted either as stratabound syngenetic deposits remobilized and concentrated during Variscan collision (Zucchetti, 1958; Schneider,

1972; Bakos et al., 1990), or syn-collisional thrust-hosted deposits (Conti et al., 1998), were most likely formed during synorogenic extension of the Variscan crust. The corresponding shear zone may therefore be regarded as a larger equivalent of the Sarlande shear zone. These features point to the importance of extensional brittle-ductile mineralising shear zones in the Variscan belt of Western Europe. Similar economically important structures may also occur in other collisional belts worldwide.

6. Conclusions

New evidence presented here shows that extensional deformation assisted by hydrothermal fluids has occurred within the brittle-ductile transition. The hydrothermal fluids originated from mid-crustal granites and were driven to and accumulated near the boundary between brittle and ductile crusts, leading to the development of a brittle-ductile transition zone in which intense fluid-rock interactions occurred. Crustal permeability inherited from compressional tectonics and metamorphism drives the fluid flow towards the transition zone. In a setting of crustal-scale extension, the progressive development of a brittle-ductile altered zone favours the growth of low-angle mineralized shear zones due to its low strength. Normal slip along shear zones accommodates part of crustal extension by producing footwall domes in the cores of which deep-seated rocks may be exhumed. The fluid pressure plays a key role at various stages of shear zone growth. Taking into account the widespread discovery of late orogenic extension in young and ancient mountain belts, our results call for a reassessment of some of mineralized brittle-ductile shear zones in other belts where there may be evidence for late orogenic extension, particularly those associated with late-orogenic domes. Many examples may illustrate further how crustal-scale fluid-rock interactions may assist in facilitating extension of the continental crust.

Acknowledgments

This work has been supported by the BRGM (3D mapping and metallogeny of the French Massif Central project). This paper is also a contribution to the GeoFrance3D program. I thank Derek J. Blundell, Bob Holdsworth and Olivier Kalish for improvements of the quality of the English. Robert P. Wintsch, Anne-Marie Boullier, and two anonymous reviewers are thanked for their constructive comments on an early version of the paper.

References

Alexandrov, P., 2000. Géochronologie U/Pb et $^{40}Ar/^{39}Ar$ de deux segments de la chaîne varisque: le haut limousin et les Pyrénées orientales. PhD thesis, INPL Nancy, France, 186 p.

Allibone, A., et al., 2002. Timing and structural controls on gold mineralization at the Bogoso gold mine, Ghana, West Africa. Economic Geology 97, 949–969.

Axen, G.J., 1992. Pore pressure, stress increase, and fault weakening in low-angle normal faulting. Journal of Geophysical Research 97, 8979–8991.

Bakos, F., Carangiu, G., Fadda, S., Mazzalle, A., Valera, R., 1990. The gold mineralization of Baccu Locci (Sardinia, Italy): origin, evolution and concentration processes. Terra Nova 2, 232–237.

Bellot, J.-P., 2001. La structure de la croûte varisque du Sud-Limousin (Massif central français) et ses relations avec les minéralisations aurifères tardi-orogéniques: apport des données géologiques, gitologiques, géophysiques et de la modélisation 3D. PhD thesis, Université de Montpellier, France, 309 p.

Bellot, J.-P., 2004. Shear zone-hosted polymetallic sulphides in the South Limousin area, Massif Central, France: Remobilized sulphide deposits related to Variscan collisional tectonics and amphibolite facies metamorphism. Economic Geology 99, 819–827.

Bellot, J.-P., Lerouge, C., Bailly, L., Bouchot, V., 2003. The Biards Sb-Au bearing shear zone (Massif Central, France): an indicator of crustal-scale transcurrent tectonics guiding late Variscan collapse. Economic Geology 98, 1427–1447.

Bellot, J.-P., Roig, J.-Y., Genna, A., 2005. The Hospital coal basin (Massif Central, France): relay on the left-lateral strike-slip Argentat fault in relation to the Variscan postorogenic extension. Bulletin de la Société Géologique de France 177, 141–149.

Bouchez, J.L., Jover, O., 1986. Le Massif Central: un chevauchement de type himalayen vers l'ouest-nord-ouest. Paris, Comptes Rendus de l'Académie des Sciences 302, 675–680.

Bouchot, V., 1989. Contexte géologique et structural des minéralisations aurifères du district de St-Yrieix (Limousin, Massif Central francais). PhD thesis, Université d'Orléans, France, 284 p.

Bouchot, V., Gros, Y., Bonnemaison, M., 1989. Structural controls on the auriferous shear zones of the Saint Yrieix district, Massif Central, France: evidence from the Le Bourneix and Lauriéras gold deposits. Economic Geology 54, 1315–1327.

Burg, J.P., Bale, P., Brun, J.P., Girardeau, J., 1987. Stretching lineation and transport direction in the Ibero-Armorican arc during the siluro-devonian collision. Geodinamica Acta 1, 71–87.

Burg, J.P., Van Dendrissche, J., Brun, J.P., 1994. Syn- to post-thickening extension in the Variscan Belt of Western Europe: Modes and structural consequences. Géologie de la France 3, 33–51.

Burov, E., Jaupart, C., Guillou-Frottier, L., 2003. Ascent and emplacement of buoyant magma bodies in brittle-ductile upper crust. Journal of Geophysical Research 108, B4. April 2002JB001904.

Byerlee, J., Mjachkin, V., Summers, R., Voevoda, O., 1978. Structures developed in fault gouge during stable sliding and stick-slip. Tectonophysics 44, 161–171.

Carter, N.L., Kirby, S.H., 1978. Transient creep and semibrittle behaviour of crystalline rocks. Pure and Applied Geophysics 116, 807–839.

Cassidy, K.F., Groves, D.I., Mcnaughaton, N.J., 1998. Late archean granitoid-hosted lode-gold deposits, Yilgarn craton, Western Australia: deposits characteristics, crustal architecture and implication for ore genesis. Ore Geology Review 13, 65–102.

Chen, P., Molnar, P., 1983. The depth distribution of intracontinental and intraplate earthquake and its implications for the thermal and mechanical properties of the lithosphere. Journal of Geophysical Research 88, 4183–4214.

Chester, F.M., 1995. A rheologic model for wet crust applied to strike-slip faults. Journal of Geophysical Research 100, 13033–13044.

Cloos, E., 1955. Experimental analysis of fracture patterns. Geological Society of America Bulletin 66, 241–256.

Collettini, C., Barchi, M.R., 2002. A low angle normal fault in the Umbria region (Central Italy): a mechanical model for the related microseismicity. Tectonophysics 359, 97–115.

Colletini, C., Holdsworth, R.E., 2004. Fault zone weakening and character of slip along low-angle normal faults: insights from the Zuccale fault, Elba, Italy. Journal of the Geological Society 161, 1039–1051.

Coney, P.J., 1980. Cordilleran metamorphic core complexes: an overview. In: Crittenden, M.D., Coney, P.J., Davis, G.H. (Eds.), Cordilleran Metamorphic Core Complexes. Geological Society of America Memoir 153, pp. 7–34.

Coney, P.J., Harms, T.A., 1984. Cordilleran metamorphic core complexes: Cenozoic extensional relics of Mesozoic compression. Geology 12, 550–554.

Conti, P., Funedda, A., Cerbai, N., 1998. Mylonite development in the Hercynian basement of Sardinia (Italy). Journal of Structural Geology 20, 121–133.

Conti, P., Carmignani, L., Funedda, A., 2001. Change of nappe transport direction during the Variscan collisional evolution of central-southern Sardinia (Italy). Tectonophysics 332, 255–273.

Cox, S.F., 1995. Faulting processes at high fluid pressures: an example of fault valve behavior from the Wattle Gully Fault, Victoria, Australia. Journal of Geophysical Research 100, 841–859.

Cox, S.F., 2002. Fluid flow in mid- to deep crustal shear systems: experimental constraints, observations on exhumed high fluid flux shear systems, and implications for seismogenic processes. Earth Planets Space 54, 1121–1125.

Cox, S.F., Etheridge, M.A., Wall, V.J., 1987. The role of fluids in syntectonic mass transport, and the localization of metamorphic vein-type ore deposits. Ore Geology Reviews 2, 65–86.

Cox, S.F., Knackstedt, M.A., Braun, J., 2001. Principles of structural control on permeability and fluid flow in hydrothermal systems. Reviews in Economic Geology 14, 1–24.

Craw, D., Windle, S.J., Angus, P.V., 1999. Gold mineralization without quartz veins in a brittle-ductile shear zone, Macraes Mine, Otago Schist, New Zealand. Mineralium Deposita 34, 382–394.

Davis, G.H., 1983. Shear-zone model for the origin of metamorphic core complexes. Geology 11, 342–347.

Davis, G.H., Coney, P.J., 1979. Geological development of the Cordilleran metamorphic core complexes. Geology 7, 120–124.

Drake, M.J., Righter, K., 2002. Determining the composition of the Earth. Nature 416, 39–44.

Durney, D.W., Ramsay, J.G., 1973. Incremental strains measured by syntectonic crystal growths. In: De Jong, K.A., Scholten, R. (Eds.), Gravity and Tectonics. Wiley, New York, pp. 67–96.

Essarraj, S., Boiron, M.C., Cathelineau, M., Fourcade, S., 2001. Multistage deformation of Au-quartz veins (Lauriéras, French Massif Central): evidence for late gold introduction from microstructural, isotopic and fluid inclusion studies. Tectonophysics 336, 79–99.

Evans, J.P., Chester, F.M., 1995. Fluid-rock interaction and weakening of faults of the San Andreas system: inferences from San Gabriel fault-rock geochemistry and microstructures. Journal of Geophysical Research 100, 13007–13020.

Faure, M., 1995. Late carboniferous extension in the Variscan French Massif Central. Tectonics 14, 132–153.

Fayon, A., Andreas, M., Teyssier, C., Person, M., Vanderhaegue, O., 2004. Fluid flow and heat transfer during exhumation of metamorphic core complexes. Geological Society of America Abstract with Programs, Denver Annual Meeting, 36, p. 549.

Floc'h, J.P., 1983. La série métamorphique du Limousin central: une traverse de la branche ligérienne de l'orogène varisque, de l'Aquitaine à la zone broyée d'Argentat (Massif central français). Unpublished thesis, Université Limoges, 450 p.

Franke, W., 2000. The mid-European segment of the Variscides: tectonostratigraphic units, terrane boundaries and plate tectonic evolution. In: Geological Society, London, Special Publications, vol. 179, pp. 35–61.

Gattacceca, J., 2001. Cinématique du basin liguro-provençal entre 30 et 12 Ma. Implications géodynamiques. PhD thesis, ENSM Paris, France, 299 p.

Gaudemer, Y., Tapponnier, P., 1987. Ductile and brittle deformations in the northern snake range, Nevada. Journal of Structural Geology 9, 159–180.

Gautier, P., Brun, J.-P., 1994. Crustal-scale geometry and kinematics of late-orogenic extension in the central Aegean (Cyclades and Ewia Island). Tectonophysics 238, 399–424.

Girardeau, J., Dubuisson, G., Mercier, J.C.C., 1986. Cinématique de mise en place des ophiolites et nappes cristallophylliennes du Limousin, Ouest du Massif central français. Bulletin de la Société Géologique de France 8, 849–860.

Gratier, J.P., Favreau, P., Renard, F., 2003. Modeling fluid transfer along California faults when integrating pressure solution crack sealing and compaction processes. Journal of Geophysical Research 108, 2104, doi:10.1029/2001JB000380.

Grocott, J., Taylor, G.K., 2002. Magmatic arc fault systems, deformation partitioning and emplacement of granitic complexes in the Coastal Cordillera, north Chilean Andes (25°30′S, 27°00′S). Journal of the Geological Society, London 159. 425–443.

Gueydan, F., Leroy, Y.M., Jolivet, L., Agard, P., 2003. Analysis of continental localization induced by reaction-softening and microfracturing. Journal of Geophysical Research 108 (B2), doi:10.1029/2001JB000611.

Guillot, P.L., 1981. La série métamorphique du Bas-Limousin: de la vallée de l'Isle à la vallée de la Vézère, le socle en bordure du bassin aquitain. Unpublished thesis, Université Orléans, 391 p.

Haeberlin, Y., Moritz, R., Fontboté, L., Cosca, M., 2004. Carboniferous orogenic gold deposits at Pataz, Eastern Andean Cordillera, Peru: geological and structural framework, paragenesis, alteration, and $^{40}Ar/^{39}Ar$ geochronology. Economic Geology 99, 73–112.

Hagemann, S.G., Gebre-Mariam, G., Groves, D.I., 1994. Surface-water influx in shallow-level Archean lode-gold deposits in Western Australia. Geology 22, 1067–1070.

Hanmer, S., Corrigan, D., Ganas, A., 1996. Orientation of nucleating faults in anisotropic media: insights from three-dimensional deformation experiments. Tectonophysics 267, 275–290.

Hartz, E., Andresen, A., Andersen, T.B., 1994. Structural observations adjacent to a large-scale extensional detachment zone in the hinterland of the Norwegian Caledonides. Tectonophysics 231, 123–137.

Hayman, N.W., Knott, J.R., Cowan, D.S., Nemser, E., Sarna-Wojcicki, A.M., 2003. Quaternary low-angle slip on detachment faults in Death Valley, California. Geology 31, 343–346.

Hernández Enrile, J.L., 1991. Extensional tectonics of the toledo brittle-ductile shear zone, central Iberian Massif. Tectonophysics 191, 311–324.

Hirth, G., Tullis, J., 1994. The nature of the brittle to plastic transition in quartz aggregates. Journal of Geophysical Research 99, 11731–11748.

Holdsworth, R.E., 2004. Weak fault-rotten cores. Science 303, 181–182.

Iık, V., Seyitolu, G., Çemen, B., 2003. Ductile-brittle transition along the Alaehir detachment fault and its structural relationship with the Simav detachment fault, Menderes massif, western Turkey. Tectonophysics 374, 1–18.

Imber, J., Holdsworth, R.E., Butler, C.A., Strachan, R.A., 2001. A reappraisal of the Sibson-Scholz model: the nature of the frictional to viscous (''brittle-ductile'') transition along a long-lived, crustal-scale fault, Outer Hebrides, Scotland. Tectonics 20, 601–624.

Janecke, S.U., Evans, J.P., 1988. Feldspar-influenced rock rheologies. Geology 16, 1064–1067.

Johnston, D.H., Williams, P.F., Brown, R.L., Crowley, J.L., Carr, S.D., 2000. Northeastward extrusion and extensional exhumation of crystalline rocks of the Monashee complex, southeastern Canadian Cordillera. Journal of Structural Geology 22, 603–625.

Jolivet, L., Faccenna, C., Goffé, B., Mattei, M., Rossetti, F., Brunet, C., Storti, F., Funiciello, R., Cadet, J.P., Para, T., 1998. Midcrustal shear zones in post-orogenic extension: the Northern Tyrrhenian Sea case. Journal of Geophysical Research 103, 12123–12160.

Kolb, J., Rogers, A., Meyer, F.M., Vennemann, T.W., 2004. Development of fluid conduits in the auriferous shear zones of the Hutti Gold Mine, India: evidence for spatially and temporally heterogeneous fluid flow. Tectonophysics 378, 65–84.

Kurz, W., Neubauer, F., 1996. Deformation partitioning during updoming of the Sonnblick area in the Tauern Window (Eastern Alps, Austria). Journal of Structural Geology 18, 1327–1337.

Ledru, P., Costa, S., Echler, H., 1994. Structure. In: Keppie, J.D. (Ed.), Pre-Mesozoic Geology in France and Related Areas. Part III, The Massif Central. Springer Verlag, Berlin Heidelberg, pp. 305–323.

Lister, G.S., Davis, G.A., 1989. The origin of metamorphic core complexes and detachment faults formed during Tertiary continental extension in the northern Colorado River region, USA. Journal of Structural Geology 11, 65–93.

Logan, J.M., Dengo, C.A., Higgs, N.G., Wang, Z.Z., 1992. Fabrics of experimental fault zones: their development and relationship to mechanical behaviour. In: Evans, B., Wong, T.F. (Eds.), Fault Mechanics and Transport Properties of Rocks: A Festschrift in Honor of W.F. Brace. Academic Press, New York, pp. 33–67.

Lost, S., Bradbury, H.J., 1984. Monitoring Fluid-Rock Interactions Across a Mid-Crustal Brittle-Ductile Transition: Possible Implications for Fluid Circulation Within a Cover Thrust Belt. CNRS Meeting, Chevauchement et deformation, Toulouse-France, pp. 61–62.

Lucchitta, I., 1990. Role of heat and detachment in continental extension as viewed from the eastern basin and range province in Arizona. Tectonophysics 174, 77–114.

Lusk, J., Calder, B.O.E., 2004. The composition of sphalerite and associated sulphides in reactions of the Cu-Fe-Zn-S, Fe-Zn-S and Cu-Fe-S systems at 1 bar and temperatures between 250 and 535 °C. Chemical Geology 203, 319–345.

Matte, P., 2001. The Variscan collage and orogeny (480–290 Ma) and the tectonic definition of the Armorica microplate: a review. Terra Nova 13, 117–121.

McKeagney, C.J., Boulter, C.A., Jolly, R.J.H., Foster, R.P., 2004. 3-D Mohr circle analysis of vein opening, Indarama lode-gold deposit, Zimbabwe: implications for exploration. Journal of Structural Geology 26, 1275–1291.

Monier, G., 1980. Pétrologie des granitoïdes du Sud-Millevaches (Massif central français). Minéralogie, géochimie, géochronologie. Doctorate thesis, Université de Clermont-Ferrand, France, 288 pp.

Passchier, C.W., 1984. The generation of ductile and brittle shear bands in a low-angle mylonite zone. Journal of Structural Geology 6, 273–281.

Passchier, C.W., Trouw, R.A.J., 1996. Microtectonics. Springer, Berlin.

Porter, C.W., Foster, R.P., 1991. Multi-phase brittle-ductile deformation and the role of Archean thrust tectonics in the evolution of the Globe and Phoenix gold deposit, Zimbabwe. In: Ladeira, E.A. (Ed.), Brazil Gold'91. Balkema, Rotterdam, pp. 665–671.

Reynolds, S.J., Lister, G.S., 1987. Structural aspects of fluid-rock interactions in detachment zones. Geology, 362–366.

Rietbrock, A., Tiberi, C., Scherbaum, F., Lyon-Caen, H., 1996. Seismic slip on a low angle normal fault in the Gulf of Corinth: evidence from high resolution cluster analysis of microearthquakes. Geophysical Research Letter 23, 1817–1820.

Roberts, D., 1998. High-strain zones from meso- to macro-scale at different structural levels, Central Norwegian Caledonides. Journal of Structural Geology 20, 111–119.

Roig, J.Y., Faure, M., 2000. La tectonique cisaillante polyphasée du Sud-Limousin (Massif Central français) et son interprétation dans un modèle d'évolution polycyclique de la chaîne hercynienne. Bulletin de la Société géologique de France 171, 295–307.

Roig, J.Y., Faure, M., Ledru, P., 1996. Polyphase wrench tectonics in the southern french Massif Central: kinematic inferences from pre- and syntectonic granitoids. Geologische Rundschau 85, 138–153.

Roig, J.Y., Faure, M., Truffert, C., 1998. Folding and granite emplacement inferred from structural, strain, TEM, and gravimetric analyses: the case study of the Tulle antiform, SW French Massif Central. Journal of Structural Geology 20, 1169–1189.

Roig, J.Y., Faure, M., Maluski, H., 2002. Superimposed tectonic and hydrothermal events during the late-orogenic extension in the Western French Massif central: a structural and $^{40}Ar/^{39}Ar$ study. Terra Nova 14, 25–32.

Rossetti, F., Faccenna, C., Crespo-Blanc, A., 2005. Structural and kinematic constraints to the exhumation of the Alpujarride Complex (Central Betic Cordillera, Spain). Journal of Structural Geology 27, 199–216.

Rumble, D., Spear, F.S., 1983. Oxygen-isotope equilibration and permeability enhancement during regional metamorphism. Journal of the Geological Society, London 140, 619–628.

Schmid, S.M., Handy, M.R., 1991. Towards a genetic classification of fault rocks: Geological usage and tectonophysical implications. In: Muller, D.W., McKenzie, J.A., Weissert, H. (Eds.), Controversies in Modern Geology. Academic Press, London, pp. 339–361.

Schneider, H.J., 1972. Schichtgebundene NE-Metall- und F-Ba-La-gerstätten im Sarrabus-Gerrei-Gebiet, SE-Sardinien. I. Bericht: Zur Lagerstättenkunde und Geologie. Neues Jahrbuch für Mineralogie, Monatshefte, 529–541.

Scholz, C.H., 1988. The brittle-plastic transition and the depth of seismic faulting. Geologische Rundschau 77, 319–328.

Sibson, R.H., 1977. Fault rocks and fault mechanisms. Journal of Geological Society, London 133, 191–213.

Sibson, R.H., 1982. Fault zone models, heat flow, and the depth distribution of earthquakes in the continental crust of the United States. Seismological Society of America Bulletin 72, 151–163.

Sibson, R.H., 1996. Structural permeability of fluid-driven fault-fracture meshes. Journal of Structural Geology 18, 1031–1042.

Simpson, C., 1985. Deformation of granitic rocks across the brittle-ductile transition. Journal of Structural Geology 7, 503–511.

Smith, B., Reynolds, S.J., Day, H.W., Bodnar, R.J., 1991. Deep-seated fluid involvement in brittle-ductile deformation and mineralization, South Montains metamorphic core complex, Arizona. Geological Society of America Bulletin 103, 559–569.

Spear, F.S., Kohn, M.J., Cheney, J.T., 1999. P-T paths from anatectic pelites. Contribution to Mineralogy and Petrology 134, 17–32.

Stewart, M., Holdsworth, R.E., Strachan, R.A., 2000. Deformation processes and weakening mechanisms within the frictional-viscous transition zone of major crustal-scale faults: insights from the Great Glen Fault Zone, Scotland. Journal of Structural Geology 22, 543–560.

Tricart, P., Schwartz, S., Sue, C., Lardeaux, J.-M., 2004. Evidence of synextension tilting and doming during final exhumation from analysis of multistage faults (Queyras Schistes lustrés, Western Alps). Journal of Structural Geology 26, 1633–1645.

Tullis, J., Yund, R.A., 1992. The brittle-ductile transition in feldspar aggregates: An experimental study. In: Evans, B., Wong, T.-F. (Eds.), Fault Mechanics and Transport Properties of Rocks. Academic Press, San Diego, pp. 89–117.

Vallance, J., Boiron, M.C., Cathelineau, M., Fourcade, S., Varlet, M., Marignac, C., 2004. The granite-hosted gold deposit of Moulin de Chéni (Saint-Yrieix district, Massif Central, France): petrographic, structural, fluid inclusion and oxygen isotope constraints. Mineralium Deposita 39, 265–281.

Vidal, O., Parra, T., Trotet, F., 2001. A thermodynamic model for Fe-Mg aluminous chlorite using data from phase equilibrium experiments and natural pelitic assemblages in the 100° to 600 °C, 1 to 25 kb range. American Journal of Sciences 301, 557–592.

Wawrzyniec, T., Selverstone, J., Axen, G.J., 1999. Correlations between fluid composition and deep-seated structural style in the footwall of the Simplon low-angle normal fault, Switzerland. Geology 27, 715–718.

Wells, M.L., 2001. Rheological control on the initial geometry of the Raft River delta shear zone, western United States. Tectonics 20, 435–457.

White, S., 1976. The effect of strain on the microstructures, fabrics and deformation mechanisms in quartz. Philosophical Transactions of the Royal Society of London A283, 69–86.

White, J.C., White, S.H., 1983. Semi-brittle deformation within the Alpine fault zone, New Zealand. Journal of Structural Geology 5, 579–589.

Wibberley, C.A.J., Petit, J.P., Rives, T., 2000. Micromechanics of shear neorupture and the control of normal stress. Journal of Structural Geology 22, 411–427.

Wintsch, R.P., Christoffersen, R., Kronenberg, A.K., 1995. Fluid-rock reaction weakening of fault zones. Journal of Geophysical Research 100, 13021–13032.

Yan, D.-P., Zhou, M.-F., Song, H., Fu, Z., 2003. Structural style and tectonic significance of the Jianglang dome in the eastern margin of the Tibetan Plateau, China. Journal of Structural Geology 25, 765–779.

Ziegler, P., 1989. Evolution of Laurussia. Kluwer Academic publishers, Dordrecht/Boston/London, 102 p.

Ziegler, P.A., Cloethingh, S., Van Wees, J.-D., 1995. Dynamics of intra-plate compressional deformation deformation: the Alpine foreland and other examples. Tectonophysics 252, 7–59.

Zucchetti, S., 1958. The lead-arsenic-sulphide ore deposit of Bacu Locci (Sardinia-Italy). Economic Geology 53, 867–876.